Kinetostatic and dynamic properties of Cheope a parallel-serial manipulator

Angelo Vertuan[1], Serena Ruggeri[1], Giovanni Legnani[1]
[1]*Dipartimento di Ingegneria Meccanica e Industriale, Università degli Studi di Brescia*
E-mail: {angelo.vertuan, serena.ruggeri, giovanni.legnani}@ing.unibs.it

Keywords: manipulability ellipsoid, PKM, contour tracking.

SUMMARY. This work discusses the kinetostatic and dynamic properties of a new reconfigurable parallel-serial hybrid manipulator with redundant actuators carrying a serial wrist with 3 degrees of freedom (dof). The parallel part can be easily reconfigured with a simple disassembly and reassembly procedure to obtain different configurations. The paper focuses on the kinematics of the parallel structure solving the direct and the inverse kinematics of the 3 dof configuration and analyzing the singularities. The evaluation of some kinetostatic performance indices of the 3 dof configuration and some experimental result will be also presented.

1 INTRODUCTION

In the last decades many Parallel Kinematic Machines PKM have been designed and built to face the new demanding requests of industries and service companies. The good kinematic properties of these manipulators promote them as good candidates in many application fields. However, since their working space and the rotation of the moving platform are generally small, the PKM are sometimes improved adding a serial wrist, obtaining a parallel-serial hybrid manipulator [1], [2], [3], or using actuation redundant schemes [4] or kinematic redundant schemes [5].

This paper discusses the kinetostatic properties of the parallel part of Cheope, a reconfigurable hybrid manipulator. Cheope was initially designed as a robot manipulator for surgical applications [6]. The parallel architecture assures the high stiffness [7], simple structure [8] but limited dexterity.

For this reason Cheope was designed with an hybrid structure: a parallel manipulator having a serial wrist fixed on the mobile platform. The parallel part is reconfigurable to obtain special performances in particular situations and the serial wrist has 2 rotations plus a redundant translation to perform rapid and precise linear motion. The design of the manipulator has been optimized to take advantage of both kinematic architectures, to avoid singularities and to have an approximate isotropic behavior in the center of the workspace [9].

High performance components and the design of the Cheope parallel structure make it suitable for other application fields such as fast pick and place, machining and assembly tasks. The aim of this paper is to describe the kinematic characteristics of "Cheope" with special attention to its parallel reconfigurable part. At first all the possible different configurations are brefely shown and then the 3 dof configuration is analyzed solving the forward and inverse kinematics and so the kinetostatic performances are investigated by using performance ellipsoids. Experimental results of an hybrid force-velocity controlled task are also briefly discussed.

2 THE RECONFIGURABLE ARCHITECTURE

Cheope has an hybrid kinematic structure composed by a Parallel Kinematic Machine (PKM) carrying on the mobile platform a serial chain $\underline{R}\ \underline{R}\ \underline{P}$ (see fig.1). The symbol $\underline{R}$ indicates actuated revolute joints and $\underline{P}$ prismatic ones while the symbol S denotes unactuated spherical joints used in the parallel part. The parallel structure is composed by 4 actuated prismatic joints (linear motors)

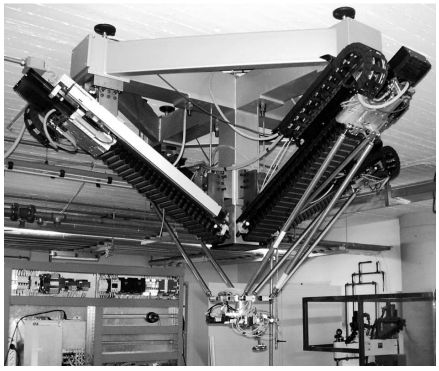

Figure 1: The *Cheope* manipulator.

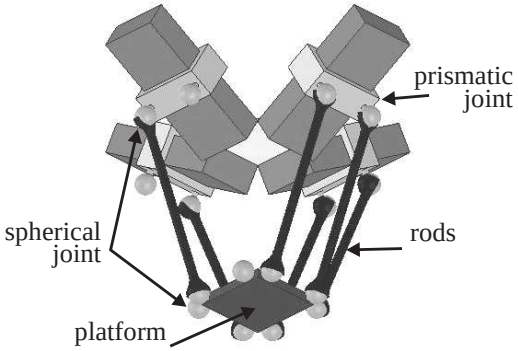

Figure 2: Parallel kinematic structure.

that lie on the edges of a square pyramidal base. Each motor can be connected to the mobile base by 0, 1 or 2 identical rods with a spherical joint at each end (fig.2). The number and the disposition of the rods can be quickly changed with simple reassembly operations. Each configuration is labelled by a string indicating the joint sequence of each "leg" (PSS in our case) and by an index indicating the number of connecting rods (1 or 2 in our case).

The 8 major configurations (figure 3) can be classified in four groups. Other configurations can be generated by symmetry and are not reported in the figure. The relevant configurations are:

(I) 3 identical $\underline{P}[SS]_2$ legs that let the mobile base have 3 degrees of freedom of pure translation (figure 3-(a)) [10];

(II) two $\underline{P}[SS]_2$ and two $\underline{P}[SS]$ chains that let the mobile base have 4 dof [11]. The legs can be assembled in 5 different geometrical configurations, see fig. 3-(b,c,d,e,f), each of them having a different rotation axis plus three translations;

(III) 7 rods shared in three $\underline{P}[SS]_2$ legs and one $\underline{P}SS$ leg that make the system overconstrained but, if correctly controlled, the mobile platform has three translational dof (figure 3-(g));

(IV) 8 rods grouped in 4 $\underline{P}[SS]_2$ legs; the mobile platform has 3 translational dof and a double overconstrain generated by the fourth actuator (figure 3-(h)).

In this paper we focus only on the configuration (I) and we refer to them as "3 dof configuration". In this configuration only 3 prismatic joints are actuated, and each of them is connected to the mobile base by a couple of rods. Because of the chosen geometrical dimensions, each couple of rods are always parallel to each other and the mobile base can only translate inside the whole workspace, (no rotations are possible). If we limit our mobility study at first order kinematic [12], we can observe that if the centers of the four spherical joints of each $\underline{P}[SS]_2$ leg lie in a plane (planar parallelogram), virtual rotations of the mobile base around any axes orthogonal to parallelogram plane are denied. As a whole, we have three linear independent planar parallelograms and so three independent directions of rotation are prevented. We conclude that the end effector can only translate. For a more detailed description of the other configurations see [13].

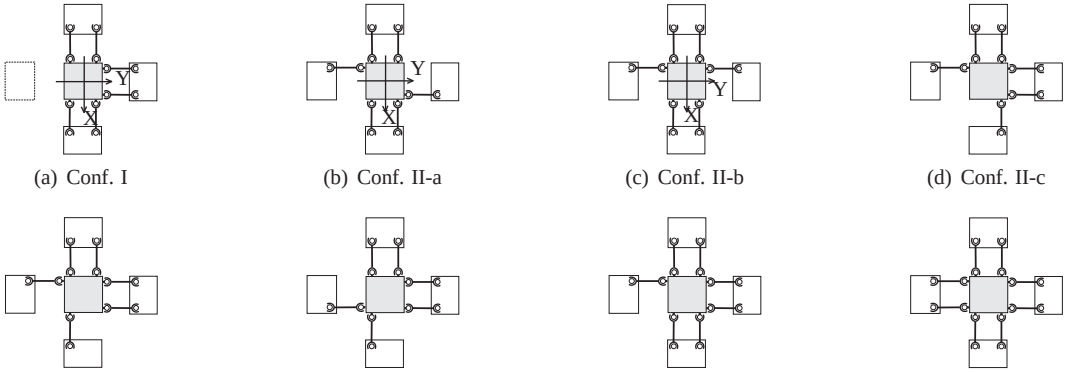

(a) Conf. I (b) Conf. II-a (c) Conf. II-b (d) Conf. II-c

(e) Conf. II-d (f) Conf. II-e (g) Conf. III (h) Conf. IV

Figure 3: All the possible isostatic (I, II) and overconstrained configurations (III, IV).

3 NOTATION

With reference to fig. 4 the following conventions have been adopted for the 3 dof configuration:

- *Rod and linear axis indices*: $i = 1 \dots 6$ identifies the rod (top view, counter-clockwise), $j = 1 \dots 3$ identifies joint prismatic axis.
- $\{0\}$ is the absolute frame. The origin is at the intersection of the axes of the prismatic joints, Z_0 vertical axis (coincident with chassis symmetry axis) and X_0 horizontal axis in the direction of prismatic joint 1;
- *l*: length of rods.
- $\mathbf{w}_j$: unit vector of the rod (or of the couple of rods) connected to $j-th$ prismatic joint.
- $\mathbf{n}_j$: unit vector of the $j-th$ prismatic joint.
- q_j: joint coordinates of $j-th$ prismatic joint.
- $\mathbf{q} = [\ q_1, \dots, q_3\ ]^T$ joint coordinates vector.
- $\mathbf{s}_3 = [\ x,\ y,\ z\ ]^T$: Tool Center Point (TCP) coordinate vector, for 3 dof configuration.

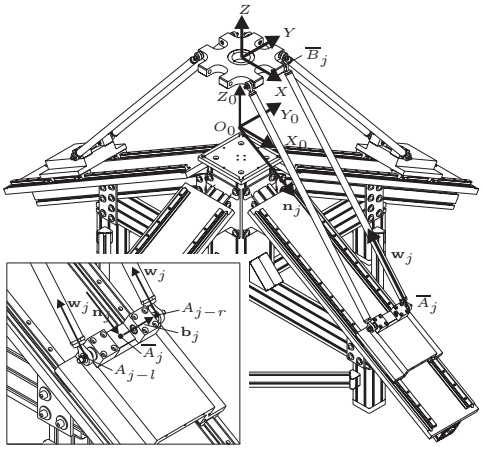

Figure 4: The adopted notation.

- $\mathbf{a}_j$, $\mathbf{b}_j$ and $\mathbf{d}_j$: vectors that lie on the platform, see figure 4 - (c,d)
- $A_i = A_{j-l}$, $A_{i+1} = A_{j-r}$ and $B_i = B_{j-l}$, $B_{i+1} = B_{j-r}$ with $i = 1, 3, 5, 7$: coordinates of the two end points of the $i-th$ (or $(i+1)-th$) rod. The subscript $j-l$ and $j-r$ mean respectively the right hand and left hand rod for the $j-th$ linear axis (see figure 4-(c,d))
- $\overline{A}_j = \frac{1}{2}(A_{j-l} + A_{j-r})$ and $\overline{B}_j = \frac{1}{2}(B_{j-l} + B_{j-r})$: mean point between the ends of a couple of adjacent rods (see figure 4-(c,d))
- $\mathbf{f}_{xyz} = [\ f_x,\ f_y,\ f_z\ ]^T$: external forces applied at the center of the platform (mobile base).
- $\mathbf{t}_{xyz} = [\ c_x,\ c_y,\ c_z\ ]^T$: external torques applied to the platform.

4 KINEMATIC ANALYSIS

The kinematic analysis has been developed writing 3 closure loop equations for each couple of adjacent rods. The loop-closure equation for the $j-th$ limb can be written along a virtual central rod which connects the points $\overline{A}_j$ and $\overline{B}_j$ (fig. 4) and it results:

$$\mathbf{s}_3 + \mathbf{a}_j - l\mathbf{w}_j - q_j\mathbf{n}_j = 0 \qquad j = 1\dots 3\ , \tag{1}$$

defining $\mathbf{c}_j(q_j) = q_j\mathbf{n}_j - \mathbf{a}_j$, from eq. (1) we have:

$$|\mathbf{s}_3|^2 - 2\mathbf{c}_j(q_j)^T\ \mathbf{s}_3 + |\mathbf{c}_j(q_j)|^2 = l^2 \qquad j = 1\dots 3\ . \tag{2}$$

The set of the three eqs.1 represents the intersection of 3 spheres; l is the radius of the spheres and $\mathbf{c}_j(q_j)$ are their centers.

4.1 Direct kinematics

$\mathbf{c}_j(q_j)$ (motors positions) are known and $\mathbf{s}_3$ (mobile base position) must be determined. To simplify the quadratic system we define the auxiliary frame $\{\mathrm{a}\}$ in which the equations of the spheres are simpler. The frame $\{\mathrm{a}\}$ has origin O_a coincident with $\mathbf{c}_1$, X_a passing trough $\mathbf{c}_2$ and the plane X_aY_a contains $\mathbf{c}_3$. In this frame the centers of the spheres are $\mathbf{c}_1 = [0,\ 0,\ 0]^T$, $\mathbf{c}_2 = [x_{c2},\ 0,\ 0]^T$, $\mathbf{c}_3 = [x_{c3},\ y_{c3},\ 0]^T$. We indicate with $\mathbf{s}_a = [\ x_a,\ y_a,\ z_a\ ]^T$ the intersection point of the three spheres expressed in the frame $\{\mathrm{a}\}$. The base position $\mathbf{s}_3$ can be estimated from the product between the rototranslation matrix $\mathbf{M}_{0a}$ (from frame $\{0\}$ to $\{\mathrm{a}\}$) and $\mathbf{s}_a$:

$$\begin{bmatrix} \mathbf{s_3} \\ \hline 1 \end{bmatrix} = \mathbf{M}_{0a} \begin{bmatrix} x_a \\ y_a \\ z_a \\ \hline 1 \end{bmatrix} \tag{3}$$

Solving the system we obtain two solutions, but only one is feasible because of the mechanical constraints of the robot. $\mathbf{s}_a$ results:

$$\begin{cases} x_a = x_{c2}/2 \\ y_a = (x_{c3}^2 + y_{c3}^2 - x_{c2}x_{c3})/(2y_{c3}) \\ z_a = \sqrt{l^2 - x_a^2 - y_a^2} \end{cases} . \tag{4}$$

The second solution is not acceptable because it correspond to a TCP (Tool Center Point) position inside the manipulator base.

4.2 Inverse kinematics

The TCP position $\mathbf{s}_3$ is known and the motor position q_j has to be determined. The solution of this problem is simple because the three relations of eq.(1) are uncoupled. Defining $\mathbf{r}_j = \mathbf{s}_3 + \mathbf{a}_j$ we have:

$$q_j = \mathbf{n}_j^T\mathbf{r}_j \pm \sqrt{(\mathbf{n}_j^T\mathbf{r}_j)^2 - \mathbf{r}_j^T\mathbf{r}_j + l^2} \qquad j = 1\dots 3 \tag{5}$$

Due to the mechanical limits only the solution with the positive sign before the radical can be accepted. Velocity and kinetostatic analysis require the knowledge of the Jacobian matrix. Deriving eq.(1) with respect to the time we get:

$$\dot{\mathbf{s}}_3 - \dot{q}_j\mathbf{n}_j = l\omega_j \times \mathbf{w}_j \quad j = 1\dots 3 \quad \text{with} \quad \frac{d}{dt}\mathbf{w}_j = \omega_j \times \mathbf{w}_j$$

where ω_j is the angular velocity of the $j-th$ rod. Projecting each equation on the rod direction $\mathbf{w}_j$, we have the relation that describes the inextensibility of the connection rods:

$$\mathbf{w}_j^T(\dot{\mathbf{s}}_3 - \dot{q}_j\mathbf{n}_j) = 0 \qquad j = 1\ldots 3 \ .$$

Defining the matrices $\mathbf{W}_3$ and $\mathbf{K}_3$ as

$$\mathbf{W}_3 = [\mathbf{w}_1\ \mathbf{w}_2\ \mathbf{w}_3] \qquad \mathbf{K}_3 = \mathrm{diag}(\mathbf{w}_1^T\mathbf{n}_1,\ \mathbf{w}_2^T\mathbf{n}_2,\ \mathbf{w}_3^T\mathbf{n}_3) \tag{6}$$

the Jacobian matrix $\mathbf{J}$ results:

$$\mathbf{W}_3^T\dot{\mathbf{s}}_3 = \mathbf{K}_3\dot{\mathbf{q}} \qquad \mathbf{J}\dot{\mathbf{s}}_3 = \dot{\mathbf{q}} \quad \rightarrow \quad \mathbf{J} = \mathbf{K}_3^{-1}\mathbf{W}_3^T \tag{7}$$

5 THE WORKSPACE

5.1 Singularities

When the manipulator is near to a singular position, its performance indexes decrease very quickly (low stiffness, oscillations, difficult control optimization etc.) and so an accurate analysis of the singularities is needed. Following the singularities analysis for parallel robots presented in

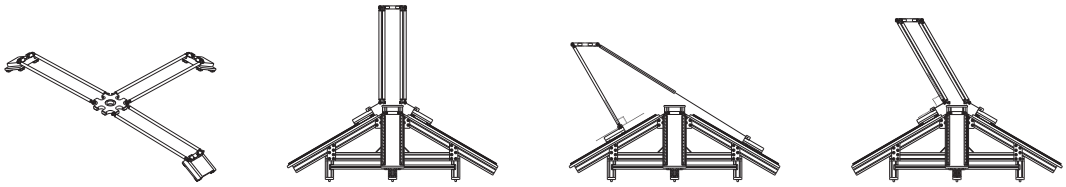

(a) (b) (c) (d)

Figure 5: Singular configurations: direct kinematic (a e b), inverse kinematic (c) and structural (d).

[14] and more extensively in Zlatanov [15] and applying it to the Cheope equations (as described in detail in [13]) we can classify the singular configurations as follows:

- *direct kinematic singularities*: if all the connection rods are coplanar (the mobile base can have an infinitesimal translation in Z direction, fig.5(a)).
- *inverse kinematic singularities*: if a connection rod is orthogonal to its prismatic joint axis (fig.5(c)), the velocity of the mobile base in the rod direction is null.
- *structural kinematic singularities*: the previous cases may occur simultaneously or two of them are parallel to each other (fig.5(b) and 5(d)).

Otherwise the kinematic structure of the "Cheope" robot has been performed to take all the possible singular configurations outside the workspace allowed by the prismatic joints limits.

5.2 Workspace

The usable workspace of the robot is limited by the closeness to singular configurations and by the endstops of the joints. The analysis of the limits imposed by the endstops of the prismatic joints of the actuators is quite simple (workspace obtained as intersection of 3 spheres), while the study of the restrictions caused by the limitations of the spherical joints is more complex. The adopted spherical joints permits a limited rotation of about ± 22 deg. This constrain results in a reduction of the reachable working space.

Figures 5.2 represents the sections of the working space of the robot for the 3 dof configuration numerically computed considering all joint limits. The working area is represented in the YZ plane for different values of the X coordinate.

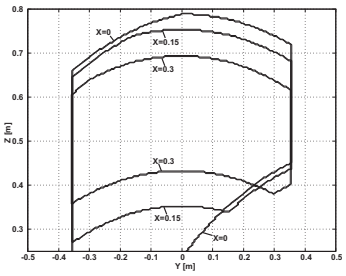

Figure 6: Workspace limits.

6 KINETOSTATIC PROPERTIES

6.1 Kinetostatic and dynamic properties

Several indices [16] have been proposed to measure the kinetostatic and the dynamic performances of the manipulator, its degree of isotropy and the distance from singularities.

Most of the adopted criteria are based on the Jacobian matrix. Other parameters to be considered are the performances of the actuators (maximum velocity and torque/force), the masses of the links and the compliance of some components. The analysis requires the evaluation of the eigenvalues and eigenvectors of a matrix which depends on the Jacobian and other dynamic parameters (masses, stiffness, actuators performances, ...).

The kinetostatic properties can be graphically represented by some performance ellipsoids introduced by Yoshikawa [17] for serial manipulators and then applied to PKMs by Gosselin et al. [18], Bhattacharya et al. [19], Merlet [20], and others. As better described in the sequel, it is possible to define force ellipsoid, velocity ellipsoid, compliance ellipsoid and mass ellipsoid each of which represents a different kinetostatic or dynamic property of the manipulator in one particular configuration. Since in our manipulator all the actuators are identical to each other, velocity and force ellipsoids can be defined by a symplified method that doesn't consider the actual value of maximum velocity and force that can be generated by each actuator.

– *Velocity ellipsoid* is defined as

$$\dot{\mathbf{s}}^T \left(\mathbf{J}^{-T}\mathbf{J}^{-1}\right)\dot{\mathbf{s}} = 1 \qquad \text{with} \qquad \dot{\mathbf{s}} = [\ \dot{x}\ \dot{y}\ \dot{z}\ ]^T \tag{8}$$

where $\dot{s}$ indicates the maximun possible velocity of the end effector in the various directions of the workspace given a maximum value of motors' velocity assumed equal to one. The Jacobian matrix correlates joints and end effector velocity and joint and end effector infinitesimal movements. This is why the velocity ellipsoid indicates also the effects on repeatibility of the end effector motion due to uncertainty of joint motion.

– Similarly *force ellipsoid* is defined as

$$\mathbf{F_s}^T \left(\mathbf{J}\mathbf{J}^T\right)\mathbf{F_s} = 1 \qquad \text{with} \qquad \dot{\mathbf{F}}_\mathbf{s} = [\ f_x\ f_y\ f_z\ ]^T \tag{9}$$

and it describes the maximum forces ($\mathbf{F_s}$) that can be exerted by the end effector in the various directions of the workspace.

– *Stiffness ellipsoid* indicates the stiffness of the robot in the work space assuming the compliance concetrated at the actuators. Indicating with k the actuator stiffness it is defined as

$$\mathbf{F_s} = \frac{1}{k}\left(\mathbf{J}\mathbf{J}^T\right)^{-1}\mathbf{ds} \qquad \text{with} \qquad \mathbf{ds} = [\ dx\ dy\ dz\ ]^T \tag{10}$$

and it describes the relation between intensity and direction of forces ($\mathbf{F_s}$) exerted at the end effector and the consequent displacement ($\mathbf{ds}$) of it. Generally we can gather that the robot is more stiff in the direction in which it can exert greater forces.

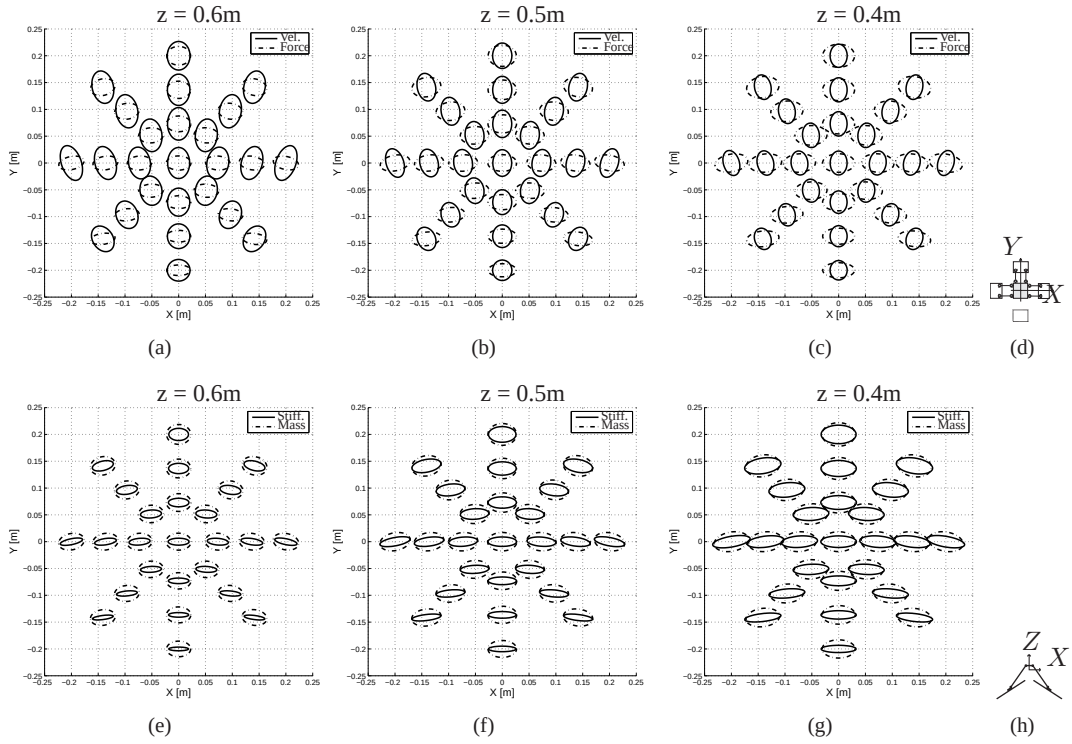

Figure 7: Manipulability force, velocity, stiffness and mass ellipsoides. The sections are referred to XY plane at different workspace z quote.

– *Mass ellipsoid* gives informations on the acceleration of the end effector in the workspace when external forces are applied to it. It is defined as

$$\mathbf{F_s} \simeq \left(\mathbf{J_e}^{-T}\overline{\mathbf{M}}\mathbf{J_e}^{-1}\right)\ddot{\mathbf{s}} \tag{11}$$

where $\mathbf{J_e}$ is an extended Jacobian and $\overline{\mathbf{M}}$ is a suitable matrix of the masses. It indicates the forces $\mathbf{F_s}$ necessary to produce an acceleration $\ddot{\mathbf{s}}$. Mass ellipsoid together with the stiffness ellipsoid could be related to vibration phenomena when the robot interacts with the environment in machining applications.

Synthetic performances indexes are also the determinant, the condition number or the singular values of $\mathbf{J}$ [21]. The condition number is defined as $c = cond(\mathbf{J}) = ||\mathbf{J}||||\mathbf{J}^{-1}||$. If the norm is defined as the maximum singular value ("spectral norm"), the condition number equals the ratio $cond(\mathbf{J}) = \sigma_{max}(\mathbf{J})/\sigma_{min}(\mathbf{J})$. The singular value σ_i represents the size of the principal axis of the ellipsoid, while $\det(\mathbf{J}) = \sigma_1 \cdot \sigma_2 \cdot \sigma_3$ is related to the volume of the ellipsoid. By virtue of the duality between kinematics and statics, σ_{min} and σ_{max} are also measures of the stiffness of the mechanism. The bigger the volume, the more rigid the manipulator is. The mapping of the condition number c of σ_{min} and of $det(\mathbf{J})$ can be used for a rough evaluation of the usable workspace.

Figure 7 display the performance ellipsoids of "Cheope" in some locations of the workspace. Due to mechanical simmetry with respect to Y axis (figure 7(d) and 7(h)), the kinetostatic performances of the manipulator are also symmetrical with respect to the same axis.

The meaning of the ellipsoids is briefly expalined as follows. In figure 7 the axes of the force ellipses are nearly parallel to the reference axes X and Y and the length of the force ellipses in the X direction is bigger than the one in the Y direction. This means that the force that the manipulator can exert in the X direction is bigger than the one it can exert in Y direction. This behaviour does not change with the quote Z. Similarly the velocity that the manipulator can reach in Y direction is bigger than the one the manipulator can reach in X.

Figure 7 also shows the mass and the stiffness ellipses. From that figure it is quite evident that the equivalent mass in X direction is bigger than the one in Y direction, but the differences are not so big. On the contrary the stiffness in X and Y are pretty different and in Y direction the manipulator has a lower stiffness (greater compliance). Since equivalent mass and stiffness vary significantly with the direction we can predict that, when the manipulator is in contact with the environment, its dynamic behauviour depends on the direction of the contact. A simmetry whith respect to the Y direction is also present. Observing the figures at different z position it's easy to note that going toward a singular position (rod parallel to each other at maximum z quote, see fig. 5(b)) mass and stiffness decrease with consequent deterioration of the performances.

7 A PRACTICAL APPLICATION: ANALYSIS OF THE CONTOUR TRACKING

An application has been developed to verify the considerations about the kinematic and the dynamic properties of the manipulator. The developed application is the contour tracking using a force sensor mounted at the robot's end effector. For these applications a force controller or an hybrid force/position/velocity controller is needed [22].

In this application it is necessary to maintain the contact of the TCP (Tool Center Point) with the surface of an object of unknown shape while the manipulator is moving along the piece contour. It is similar to a blind man which is able to move in a room because with his hands he touches the environment to sense the wall and the obstacles to identify their position and shape. During the contour tracking task the robot controls the tangential velocity and the normal force with respect to the surface of the object. The manipulator detects the correct normal and tangential direction using the data collected by the force sensor. For this kind of applications it is useful to use the *task frame* formalism as suggested firstly by De Schutter [23]. In our specific application we have contourned a round steel disk of $14cm$ diameter of placed in the center of the XY plain at $50cm$ along the Z direction. Observing figure 8 and 9 it's possible to correlate the performance ellipsoides with the dynamic behavior of the manipulator. The force error is worse when the normal of the object is parallel to the minor axis of the stiffness and mass ellipsoides.

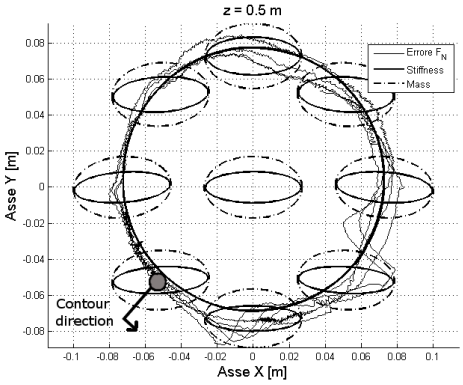

Figure 8: Contour tracking test: shape of the object, force error and performances ellipses (stiffness and mass).

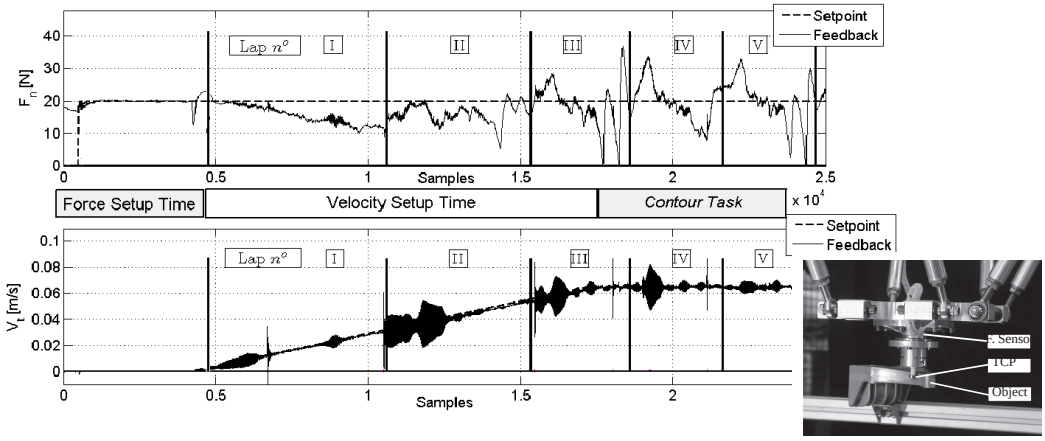

Figure 9: Force and velocity response versus time during contour tracking (sampling time $400Hz$). The first three laps are executed with increasing speed which stays constant in laps IV and V.

8 CONCLUSIONS

The paper presents the main kinetostatic characteristics of "Cheope", a reconfigurable parallel-serial hybrid manipulator. Particular attention is paid to the 3 dof translation configuration: forward and inverse kinematic problems have been solved and performances have been deeply analized with the help of the performance ellipsoids. The manipulator is nearly isotropic from a kinematic point of view for a great part of its workspace. However from a dynamic point of view the manipulator presents an anisotropic behaviour. The effect of dynamics and anisotropy can be observed in applications interacting with the environment as the contour tracking task that has been successfully attempted. The choice of high performance mechanical components (mainly the linear motors) allowed to achieve good dynamical performances. The robot Cheope, initially designed as a prototype for medical application, can be conveniently applied also in different fields (machining, surface finishing, assembly tasks, etc.).

REFERENCES

[1] R. Ricard and C. Gosselin, "On the development of hybrid planar manipulators," in *Proc. 36th IEEE Midwest Symposium on Circuits and Systems*, vol. 1, Detroit, USA, 16-18 August 1993, pp. 398–401.

[2] T. K. Tanev, "Kinematics of a hybrid (parallel-serial) robot," *Mech Mach Theory*, vol. 35, pp. 1183–1196, 2000.

[3] H.-S. Choia, C.-S. Hana, K. young Lee, and S.-H. Lee, "Development of hybrid robot for construction works with pneumatic actuator," *Automat Constr*, vol. 14(4), pp. 452–459, August 2005.

[4] S. Kock and W. Shumacher, "A parallel x-y manipulator with actuation redundancy for high-speed and active-stiffness applications," in *Proc. of the 1998 IEEE International Conference on Robotics and Automation*, May 1998, pp. 2295–2300.

[5] J. Wang and C. M. Grosselin, "Kinematic analysis and design of kinematically redundant parallel mechanism," *Journal Mech Design*, vol. 126, no. 1, pp. 109–118, January 2004.

[6] D. Tosi, G. Legnani, R. Adamini, H. Giberti, and P. Righettini, "Progetto di *"cheope"*: un manipolatore ridondante ibrido parallelo-seriale," in *AIMETA 2003*, Ferrara, Italy, 9-12 Sept. 2003.

[7] L. Tsai, *Robot Analysis: The Mechanics of Serial and Parallel Manipulators*. Wiley, 1999.

[8] F. Gao *et al.*, "New kinematic structures for 2-,3-,4- and 5-dof parallel manipulator designs," *Mech Mach Theory*, vol. 37(11), pp. 1395–1411, Nov. 2002.

[9] T. Huang, D. Whitehouse, and J. Wang, "The local dexterity, optimal architecture and design criteria of parallel machine tools," *Annals of the CIRP*, vol. 47, no. 1, pp. 347–351, 1998.

[10] M. Hebsacker, T. Treib, O. Zirn, and M. Honegger, "Hexaglide 6 dof and triaglide 3 dof parallel manipulators," *In: C.R. Bor, L. Molinari-Tosatti and K.S. Smith, Editors, Parallel Kinematic Machines: Theoretical Aspects and Industrial Requirements, Springer-Verlag*, pp. 345–355, 1999.

[11] L. Rolland, "The manta and the kanuk: Novel 4-dof parallel mechanisms for industrial handling," in *Proc. ASME Dynamic Systems and Control Division, IMECE'99 Conference*, vol. 67, Nashville, USA, 14-19 November 1999, pp. 831–844.

[12] R. S. Ball, *A Treatise on the Theory of Screws*. Cambridge University Press, 1900.

[13] A. Vertuan, G. L. nad R. Adamini, D. Tosi, and N. Pedrocchi, "Performance analysis of a reconfigurable redundant parallel manipulator," in *Reconfiugrable Mechanisms and Robots*. London: ASME/IFToMM Int. Conf. on Reconfigurable Mech. and Robots(ReMAR 2009), jun 2009, pp. 593–601.

[14] G. Legnani, *Robotica industriale*. Milano: Editrice Ambrosiana, 2003.

[15] D. Zlatanov, R. Fenton, and B. Benhabib, "Identification and classification of the singular configurations mechanism," *Mech Mach Theory*, vol. 33, no. 6, pp. 743–760, 1998.

[16] C. Gosselin, "Stiffness mapping for parallel manipulator," in *IEEE T Robotic Autom*, vol. 6, no. 3, 1990, pp. 377–382.

[17] T. Yoshikawa, *Foundations of robotics: Analysis and control*. MIT Press, 1990.

[18] C. Gosselin and J. Angeles, "Singularity analysis of closed loop kinematic chains," in *IEEE T Robotics Autom*, vol. 6, no. 3, 1990, pp. 281–290.

[19] S. Bhattacharya, H. Hatwal, and A. Ghosh, "On the optimum design of stewart platform type parallel manipulators," *Robotica*, vol. 13, no. 2, pp. 133–140, 1995.

[20] J. Merlet, *Parallel robots*. the Netherlands: Kluwer Academic Publishers, 2000.

[21] I. Fassi, "Analysis and design of parallel manipulators for manufacturing," Ph.D. dissertation, Politecnico di Milano, 2000.

[22] B. Siciliano and L. Villani, *Robot Force Control*. Boston: Kluwer Academic Publishers, 1999.

[23] J. D. Schutter, "Compliant robot motion: task formulation and control," Ph.D. dissertation, Katholieche Universiteit Leuven, Belgium, 2000.